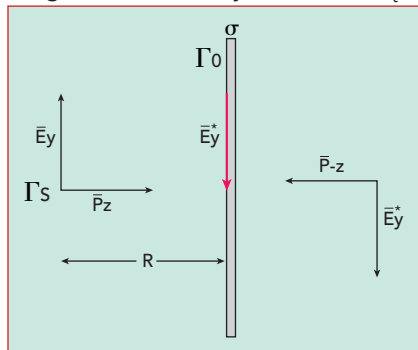


# Single Antenna Measurement Using Image Reflection

Michael D. Hillbun  
Diamond Engineering

A methodology for determining antenna gain and pattern parameters uses the image created by a conductive plane located at a desired reference position relative to the antenna phase center. The measurement consists of two states. The first is bore-sight perpendicular  $S_{11p}$  and the second is free space  $S_{11fs}$ . The original work was derived by Edward Purcell.<sup>1</sup> Later, Lee and Baddour<sup>2</sup> refined the derivation to include a finite mismatch between the antenna and its feed. The method they used involved taking several measurements over distance and performing a best fit line; reflection phase was not considered. Now that modern vector network analyzers (VNAs) can include phase, accuracy is enhanced and the separation is fixed. In addition to antenna under test (AUT) gain, phase can also be calculated such that a full 2-port [S] matrix can be determined.

It is well established that boundary conditions on metallic surfaces require  $E_t = 0$ . An incident electric field is made zero on the surface by setting up currents equal in amplitude but with opposite phase (see **Figure 1**). The induced currents are equivalent to the inverted image on the opposite side of the conductor surface and reflect off the surface with the same pattern as the incident wave.<sup>1</sup> Equivalently, the field incident on a perfect conductor generates a conjugate field at the surface to maintain the tangential boundary condition  $E_t =$



▲ Fig. 1 Field incident on a perfect conductor.

0, which generates an image at the same distance on the opposite side.

The original work began with the Friis Equation<sup>3</sup>

$$P_r = G_{Tx} G_{Rx} P_{Tx} \quad (1)$$

The reflected wave undergoes the same path loss so that the reflection coefficient at the source is

$$\Gamma_s = \bar{\Gamma}_0 \left( \frac{\lambda}{4\pi 2R} \right) \bar{G} \quad (2)$$

where all variables are linear vectors. R is multiplied by 2 to include the round trip and  $\Gamma_0$  is the reflective surface. If the source reflection is  $\Gamma_s$ , then the transmit field is

$$\bar{E}_{tx} = \bar{E}_y (1 - |\bar{\Gamma}_s|^2)^{\frac{1}{2}} \quad (3)$$

and the field received at the source is

$$\bar{E}_{Rx} = \bar{E}_{tx} \bar{\Gamma}_0 \left( \frac{\lambda}{8\pi R} \right)^2 (1 - |\bar{\Gamma}_s|^2) |\bar{G}|^2 \quad (4)$$

It is assumed  $\bar{G}$  and path loss are linear vectors. The  $\bar{E}_{Rx}$  vector lin-

early combines with the source mismatch so that

$$\bar{E}_{Rx}' = \bar{E}_{Tx} \bar{\Gamma}_s - \bar{E}_{Rx} \quad (5)$$

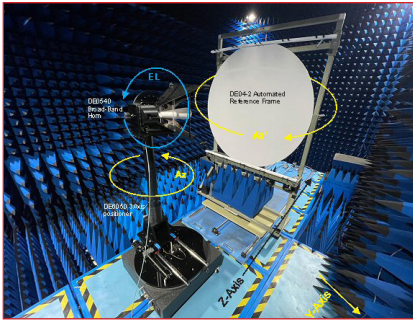
$$= \bar{E}_{tx} \bar{\Gamma}_s - \bar{E}_{tx} \left( \frac{\lambda}{8\pi R} \right)^2 (1 - |\bar{\Gamma}_s|^2) \bar{\Gamma}_0 |\bar{G}|^2 \quad (6)$$

The ratio  $\frac{\bar{E}_{Rx}}{\bar{E}_{Tx}} = \bar{\Gamma}_s$  forms the match vector due to the received reflection. While Equation (4) is a primary reflection, the higher order reflections are ignored imposing the condition  $|\bar{G}_L| \ll 1$ .

Solving Equation (6) for gain<sup>2</sup> gives

$$\bar{G} = \frac{1}{\bar{\Gamma}_0} \sqrt{\frac{\bar{\Gamma}_s - \bar{\Gamma}}{1 - |\bar{\Gamma}_s|^2}} \left( \frac{8\pi R}{\lambda} \right)^2 \quad (7)$$

It should be mentioned that all reflection quantities are vectors or Equation (7) will not be accurate.<sup>4</sup> The vector difference between the source and measurement reflection yields the AUT gain and phase referenced from the AUT connector and phase center. Equation (7) includes the conductive surface conductivity



▲ Fig. 2 Image reflection setup.

$\sigma$ . The surface reflection is given by

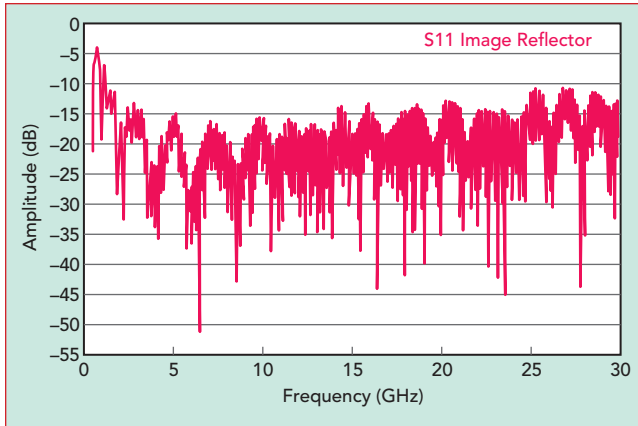
$$\bar{\Gamma}_0 = \sqrt{\frac{8\epsilon_0\omega}{\sigma}} - 1 \quad (8)$$

For high conductivity,  $\bar{\Gamma}_0 \rightarrow -1$ .

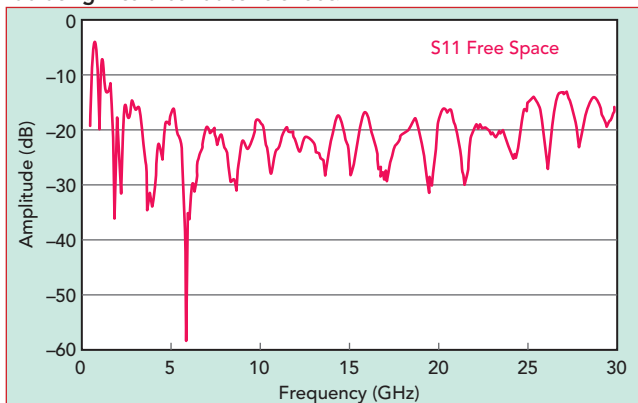
For our measurements the conductive surface is aluminum with  $\sigma = 3.5e7$  S/M and Equation (8) yields

$$\bar{\Gamma}_0 = \sqrt{\frac{50.265(8.854e^{-3})f}{3.5e7}} - 1 = 1.107e^{-4}\sqrt{f} - 1 \quad (9)$$

Where f is in GHz.



▲ Fig. 3 Measured  $|S_{11}|$  of the DE0540 horn at boresight and radiating into a conductive sheet.



▲ Fig. 4 Measured  $|S_{11}|$  of the DE0540 horn with absorber between the horn and conductive sheet.

At 10 GHz,  $\bar{\Gamma}_0 = -0.9996$  or 0.003 dB. Equation (7) has a phase component determined by  $\frac{1}{\bar{\Gamma}_0}$  and  $\sqrt{\bar{\Gamma}_s - \bar{\Gamma}}$ .

Equation (8) demonstrates that the sheet reflection loss is negligible as would be the angle deviation from 180 degrees so the AUT phase is entirely determined by the difference between the source reflection and the measured reflection. The resulting gain is

$$\bar{G} = |S_{21}|e^{j\phi} \quad (10)$$

where

$$\phi = \tan^{-1} \frac{\text{Im}\left(\frac{1}{\bar{\Gamma}_0}\sqrt{\bar{\Gamma}_s - \bar{\Gamma}}\right)}{\text{RE}\left(\frac{1}{\bar{\Gamma}_0}\sqrt{\bar{\Gamma}_s - \bar{\Gamma}}\right)} \quad (11)$$

$$\bar{S} = \begin{bmatrix} \Gamma & |S_{21}|e^{j\phi} \\ |S_{21}|e^{j\phi} & \Gamma \end{bmatrix} \quad (12)$$

Equation 10 represents the system magnitude and phase. If it is assumed that the AUT is lossless, then  $S_{11} = S_{22}$  where  $S_{11}$  is relative to a 50 ohm source and  $S_{22}$  relative to a 377 ohm load. To establish an [S] matrix for the AUT, the phase center must be known

relative to the connector. The AUT shown in **Figure 2** uses a lens that also serves to maintain a somewhat constant phase center location. This is measured using a least squares convergence algorithm for phase center offset (PCO) determination. The AUT measured  $|S_{21}|$  data is given phase, based on the PCO value. Equation (7) is replaced with

$$\bar{G} = \left| \frac{1}{\bar{\Gamma}_0} \sqrt{\frac{\bar{\Gamma}_s - \bar{\Gamma}}{(1 - |\bar{\Gamma}_s|^2)}} \left( \frac{8\pi R}{\lambda} \right)^2 \right| e^{j \frac{2\pi(\text{PCO})}{\lambda}} \quad (13)$$

To calculate  $S_{22}$  it is necessary to transform  $S_{11}$  from 50 ohms to 377 ohms. These types of transformations were originally derived by G. Bodway<sup>5</sup> as

$$S'_{11} = \frac{A_1^* \left( (1 - \bar{\Gamma}_L S_{11}) (S_{11} - \bar{\Gamma}_S^*) + \bar{\Gamma}_L S_{11} S_{21}^2 \right)}{A_1 (1 - \bar{\Gamma}_S S_{11}) (1 - \bar{\Gamma}_L^* S_{22}) - \bar{\Gamma}_L \bar{\Gamma}_L^* S_{21}^2} \quad (14)$$

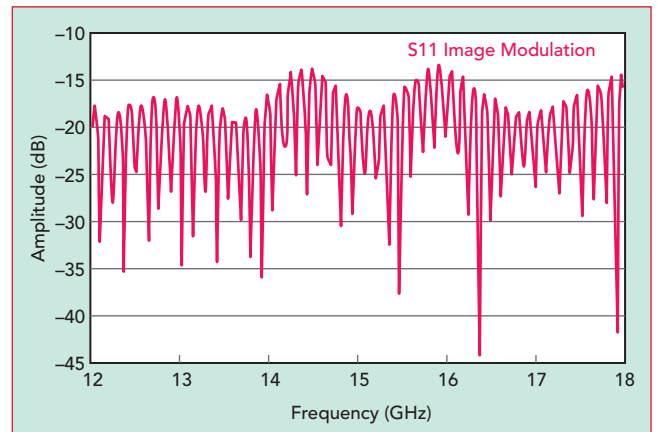
$$\text{where } A_1 = \frac{(1 - \bar{\Gamma}_S^*)}{|1 - \bar{\Gamma}_S|} (1 - |\bar{\Gamma}_S|^2) \quad (15)$$

and

$$\Gamma_s = \frac{Z_L - Z_S}{Z_L + Z_S^*} = \frac{377 - 50}{377 + 50} = .765 \quad (16)$$

and

$$A_1 = \frac{(1 + .765)}{(1 - .765)} (1 - .765^2) = 3.127 \quad (17)$$



▲ Fig. 5 Modulation of the AUT image reflection.

With the previous assumptions the antenna scattering matrix may be written as

$$[\bar{S}] = \begin{bmatrix} S_{11} & \left| \frac{1}{\bar{\Gamma}_0} \sqrt{\frac{\bar{\Gamma}_S - \bar{\Gamma}}{1 - |\bar{\Gamma}_S|^2}} \left( \frac{8\pi R}{\lambda} \right)^2 e^{j\frac{2\pi(\text{POC})}{\lambda}} \right| \\ \left| \frac{1}{\bar{\Gamma}_0} \sqrt{\frac{\bar{\Gamma}_S - \bar{\Gamma}}{1 - |\bar{\Gamma}_S|^2}} \left( \frac{8\pi R}{\lambda} \right)^2 e^{j\frac{2\pi(\text{POC})}{\lambda}} \right| & \frac{A_1^* \left[ (1 - \bar{\Gamma}_L S_{11}) (S_{11} - \Gamma_S^*) + \bar{\Gamma}_L S_{11} S_{21}^2 \right]}{A_1 (1 - \bar{\Gamma}_S S_{11}) (1 - \bar{\Gamma}_L^* S_{22}) - \bar{\Gamma}_L \bar{\Gamma}_L S_{21}^2} \end{bmatrix} \quad (18)$$

## VERIFICATION MEASUREMENTS

Verification is performed on a very broadband (500 MHz to 30 GHz) reference horn. The image reflection

setup uses a Diamond Engineering DE0540 horn antenna and an aluminum sheet at distance R (see Figure 2). Antenna gain and phase is determined from  $S_{11}$  measurement.

The phase center is determined to be 228.6 mm.

The gain of the AUT ranges from 3 to 23 dB. The conductive surface is set perpendicular to the AUT using a laser and an optically flat mirror. The sequence is to first measure the AUT  $S_{11}$  magnitude and phase di-

rectly pointed into the surface. Then the measurement is repeated after the absorber is placed between the surface and the horn, nearer the horn. **Figures 3** and **4** show the measurement results.

A magnified view of Figure 3 (see **Figure 5**) reveals the modulation of the AUT match profile. Since the reflection repeats every half wavelength, the distance between the source and mirror is:

$$R = \frac{c}{2\Delta f} = 1.25M \quad (19)$$

The reflection ripple in Figure 5 is easily filtered using a moving average. The number of points should be large enough to include at least three points in a single reflection cycle. The number of measurement points over the bandwidth generates the following measurement frequency steps:

$$\Delta f_s = \frac{BW}{n} \quad (20)$$

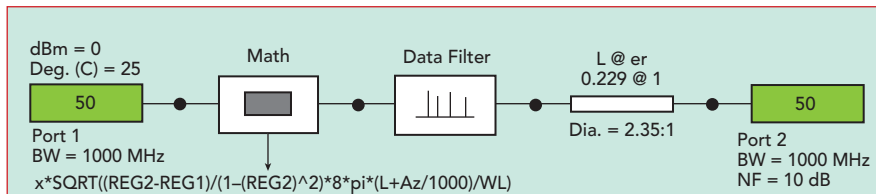
where BW is the measurement bandwidth and n is the number of measurement points.

From Figure 5, the path generates a reflection ripple of 133.3 MHz. If the measurement spanned 1 to 30 GHz, then the minimum number of measurement points would be  $\frac{29}{133} \times 3$  or 654. The measurements in this work use 2001 points.

Applying Equation (13) to Figures 3 and 4 and performing the moving average yields **Figure 6**.



▲ Fig. 6 Measured image (red) and 3-point (green) gain.



▲ Fig. 7 Schematic construct used to calculate  $S_{21}$  and  $S_{22}$ .

## S-Parameter Determination

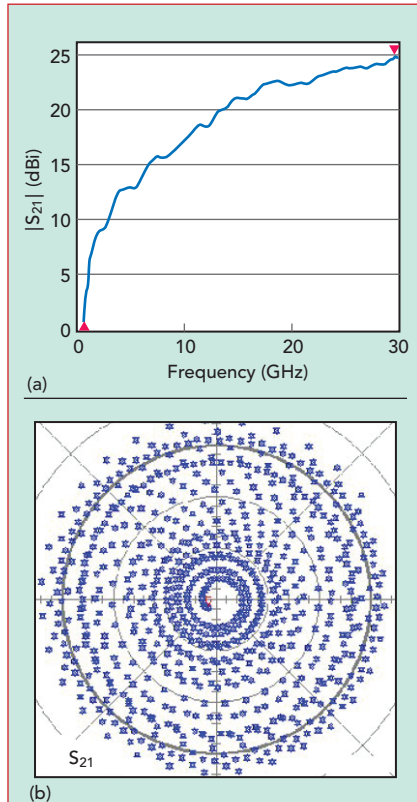
Measurement data is processed through a schematic construct (see **Figure 7**) enabling Equation (18) to be calculated. **Figure 8** shows the complex  $S_{21}$  polar plot.  $S_{22}$  (see **Figure 9**) is calculated from Figure 7 by changing the output impedance from 50 to 377 ohms. Using the calculated results from Figures 8 and

9 and the measured  $S_{11}$  completes the [S] matrix for the AUT.

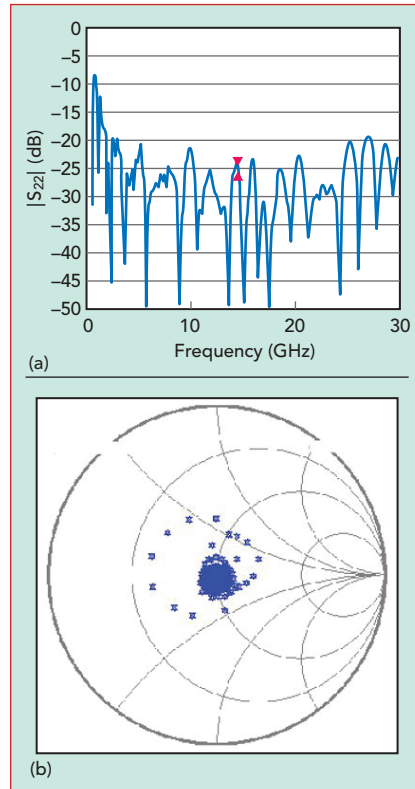
## BEAM MEASUREMENTS

The AUT is mounted on a full spherical positioner and laser bore-sight aligned with the conductive surface (see Figure 2). The movement extents are set to beam scan AZ/EL  $\pm 15$  degrees in 0.5 degree

steps. The required measurement dynamic range must accommodate the 15-degree beam width. To estimate the dynamic measurement range, the time domain can be used with a sufficient number of points. **Figure 10** shows a dynamic range of almost 45 dB. Beam measurements (see **Figure 11**) are plotted for four test frequencies.



▲ Fig. 8  $|S_{21}|$  (a) and linear polar  $S_{21}$  (b) responses.



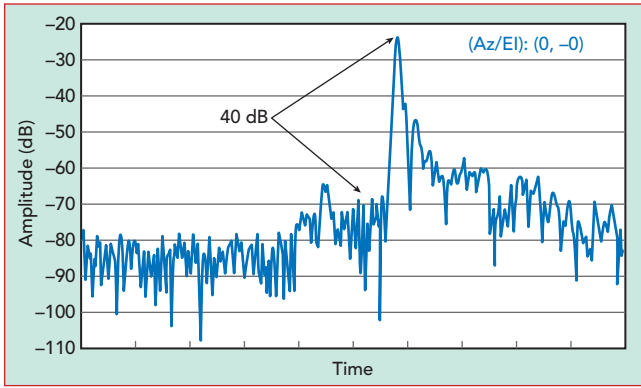
▲ Fig. 9  $|S_{22}|$  (a) and linear polar  $S_{22}$  (b) responses looking into free space (377  $\Omega$ ).

## ACCURACY CONSIDERATIONS

The ratio of measurement wavelength to reflector size sets the lowest frequency that can be measured accurately. Careful inspection of Figure 6 shows that for frequencies below 1 GHz, the image gain is much higher than the 3-point gain. At 200 MHz the wavelength (59 in.) is larger than the 48-in. reflector. Inspection of Equation (7) reveals the possibility that as  $\Gamma$  becomes smaller, the source reflection dominates the calculation giving rise to a possible larger gain value depending on phase.

$$\bar{G} \sim \sqrt{\Gamma_S - \Gamma} \quad (21)$$

**Figure 12** shows gain measured at 1 and 3 meters. A 5 dB gain error exists at 500 MHz. For a 48-in. square mirror this results in two wavelengths. As the frequency increases the error decreases to be negligible at about 2 GHz, and at 1 GHz the error is -1.2 dB. The vector ratio of the two traces represents the measurement error between 1 meter and 3 meters (see **Figure 13**). Ignoring edge diffraction, the



▲ Fig. 10 AUT time domain response.

forward  $S_{21}$  vector adds to the reflected  $S_{21}$ , which is proportional to  $W/L$  where  $W$  is the width or height of the reflector and  $L$  the path length. That proportionality is expressed as

$$S'_{21} = S_{21} + k * L \frac{\lambda}{W} \quad (22)$$

From Equation (22), the smaller  $\frac{\lambda}{W}$  the less error is present. The constant,  $k$ , may be determined from a data set where it can be assumed  $L$  is small enough to ensure accuracy, 1 meter in this example. The corrected data then becomes

$$S'_{21} = S_{21} - k * L \frac{\lambda}{W} \quad (23)$$

When Equation (23) is solved for  $k$ ,

$$k = (S_{21} - S'_{21}) + \frac{W}{\lambda L} \quad (24)$$

While a least squares algorithm would be most useful for the determi-

nation of  $k$ , a simple value can be determined by adjusting  $k$  until the lowest frequency  $S_{21}$  at 3 meters matches  $S_{21}$  at 1 meter. This is applied to data of Figure 13. **Figures 14 and 15** plot the results with  $k = 3.8$ .

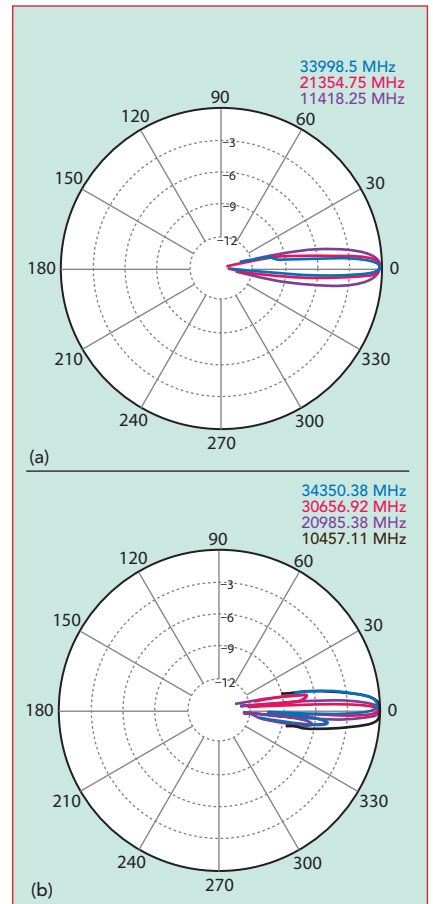
## CONCLUSION

The work of Purcell has been re-derived in vector form

to take advantage of a modern VNA's vector calibration capabilities. The resulting derivation is in good agreement with the classical 3-point method. The methodology enables antenna phase determination and a resulting S-parameter matrix. The matrix can then be used in system simulators to determine antenna bit rate error versus pointing angle. The reflection method has the advantage that only a single antenna is required; however, limitations determined by the wavelength to reflector ratio are not addressed here. The measurement is real-time, non-invasive and enables rapid antenna calibration with only a single port  $S_{11}$  measurement. It is shown that accurate measurements can be made down to two wavelengths (half the reflector width/height). ■

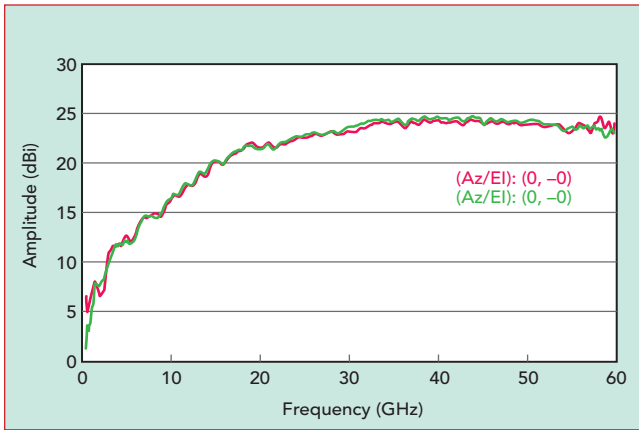
## ACKNOWLEDGMENTS

The author wishes to express his

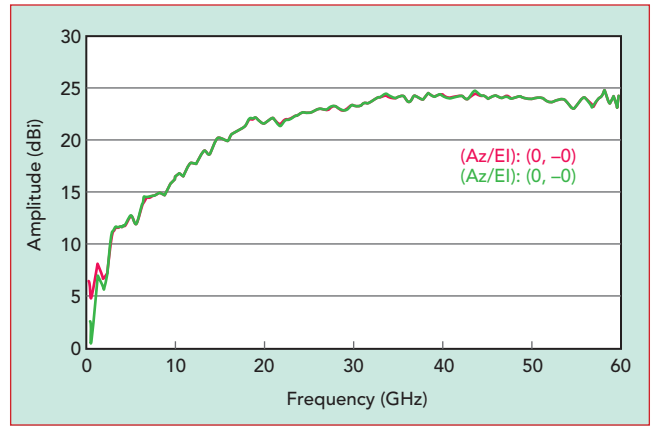


▲ Fig. 11 Elevation (a) and azimuth (b) beam measurements at several frequencies.

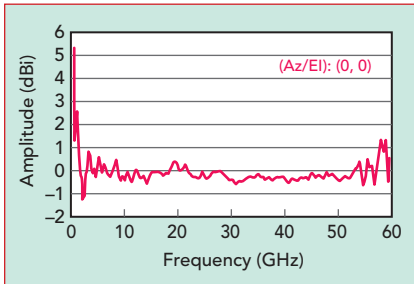
thanks and appreciation to Diamond Engineering Inc. CEO James Matthew Martin and design engineer Joshua Taylor for their valuable support and contributions without which this effort would not have been possible.



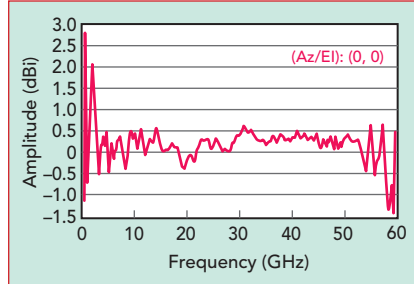
▲ Fig. 12 DE0540 horn antenna gain vs. frequency with a 48-in. reflector at 1 m (red) and 3 m (green).



▲ Fig. 14 DE0540 horn antenna gain vs. frequency with a 48-in. reflector at 3 m (red) and with correction (green).



▲ Fig. 13 DE0540 horn antenna 1 and 3 m differential gain with a 48-in. reflector.



▲ Fig. 15 DE0540 horn antenna 1 and 3 m differential gain with a 48-in. reflector and correction.

## References

1. E. M. Purcell, *A Method for Measuring the Absolute Gain of Microwave Antennas*, Radiation Laboratory, Massachusetts Institute of Technology, Report No. 41-9, 1943.
2. R. Q. Lee and M. F. Baddour, "Absolute Gain Measurement Method Under Mismatched Condition," *IEEE International AP-S Symposium*, June 1987.
3. T. G. Hickman and R. A. Heaton, "Measurement of Gain," *Microwave Antenna Measurements-NSI-MI*, Scientific Atlanta, 1969, pp. 227-268, Web. [www.nsi-mi.com/images/PDFs/Microwave\\_Antenna\\_Measurements.pdf](http://www.nsi-mi.com/images/PDFs/Microwave_Antenna_Measurements.pdf).
4. M. H. Hillbun, "Single Antenna Measurement using a Mirror and Time Domain," *IEEE Santa Clara Valley APS Chapter*, July 2012.
5. G. E. Bodway, *S-Parameter Circuit Analysis and Design*, Application Note 95, Hewlett Packard, 1967.